Human Molecular Genetics, 2017, Vol. 26, No. 15 2825–2837

doi: 10.1093/hmg/ddx153
Advance Access Publication Date: 31 May 2017
Original Article

ORIGINAL ARTICLE

Heterozygote galactocerebrosidase (*GALC*) mutants have reduced remyelination and impaired myelin debris clearance following demyelinating injury

Nicole J. Scott-Hewitt[1,†], Christopher J. Folts[1,‡], Jessica M. Hogestyn[1], Gavin Piester[2], Margot Mayer-Pröschel[1] and Mark D. Noble[1,*]

[1]Department of Biomedical Genetics, University of Rochester School of Medicine and Dentistry, Rochester, NY 14642, USA and [2]Department of Biochemistry, University of Rochester, Rochester, NY 14642, USA

*To whom correspondence should be addressed. Tel: +1 5852731448; Fax: +1 5852731450; Email: mark_noble@urmc.rochester.edu

Abstract

Genome-wide association studies are identifying multiple genetic risk factors for several diseases, but the functional role of these changes remains mostly unknown. Variants in the galactocerebrosidase (*GALC*) gene, for example, were identified as a risk factor for Multiple Sclerosis (MS); however, the potential biological relevance of GALC variants to MS remains elusive. We found that heterozygote *GALC* mutant mice have reduced myelin debris clearance and diminished remyelination after a demyelinating insult. We found no histological or behavioral differences between adult wild-type and *GALC* +/− animals under normal conditions. Following exposure to the demyelinating agent cuprizone, however, *GALC* +/− animals had significantly reduced remyelination during recovery. In addition, the microglial phagocytic response and elevation of Trem2, both necessary for clearing damaged myelin, were markedly reduced in *GALC* +/− animals. These altered responses could be corrected *in vitro* by treatment with NKH-477, a compound discovered as protective in our previous studies on Krabbe disease, which is caused by mutations in both GALC alleles. Our data are the first to show remyelination defects in individuals with a single mutant *GALC* allele, suggesting such carriers may have increased vulnerability to myelin damage following injury or disease due to inefficient myelin debris clearance. We thus provide a potential functional link between *GALC* variants and increased MS susceptibility, particularly due to the failure of remyelination associated with progressive MS. Finally, this work demonstrates that genetic variants identified through genome-wide association studies may contribute significantly to complex diseases, not by driving initial symptoms, but by altering repair mechanisms.

Introduction

Understanding why particular genetic changes increase the risk for development of a wide range of diseases is a topic of central medical concern. This interest has increased dramatically in recent years due to the ability of genome-wide association studies (GWAS) to greatly enhance the identification of not only infrequent, highly penetrant genetic variants of large risk but also of genetic loci that increase risk with lower degrees of penetrance.

For risk loci with low penetrance, there is generally little understanding of the biological changes that may increase the likelihood of developing particular diseases. Understanding the biological reasons why disease risk is increased is rendered still more difficult, moreover, by the recognition that unknown secondary insults [e.g. environmental or epigenetic factors (1)] may be critical in the conversion of risk to actual disease status. Elucidating the biological effects of particular genes, and the effects of relevant secondary insults, is central to converting our

†Present address: Department of Neurology, F.M.Kirby Neurobiology Center, Boston Children's Hospital and Harvard Medical School, Boston, MA 02115, USA
‡Present address: Division of Newborn Medicine, Department of Medicine, Boston Children's Hospital and Harvard Medical School, Boston, MA 02115, USA
Received: January 11, 2017. **Revised:** March 13, 2017. **Accepted:** April 7, 2017

understanding of risk factors from a mathematical problem of association to a biological understanding of the potential reasons for that association.

For several reasons, the problem of understanding the biology of genetic variants that increase the risk of particular diseases is of particular interest in respect to heterozygous carriers of mutations that cause autosomal recessive diseases. Although in its early stages, research in this field has revealed that carriers of mutations that cause the autosomal recessive lysosomal storage disorders (LSDs) of Krabbe disease (KD) and Gaucher disease (GD) are at increased risk for development of, e.g. open angle glaucoma (2) or Parkinson's disease (3–5), respectively. Although the frequency of KD and GD is very low (1:80,000-100,000), the gene frequency for heterozygous carriers of disease-causing mutations is high enough (1:125-150) (6) to represent a significant proportion of the population. These diseases also offer the experimental advantage that animal models that mimic KD and GD are readily available for study of biological alterations in heterozygous carriers of disease-causing mutations (7,8).

One example of the challenge of understanding potential biological contributions of a particular locus to increased disease risk is provided by studies on Multiple Sclerosis (MS), another disease associated with the genetic locus mutated in KD. MS, the most common autoimmune disorder affecting the central nervous system (CNS), is associated with widespread damage to myelin (the lipid-rich insulating material critical for neuronal conduction), eventual failure to repair such damage, and multiple neurological sequelae (9–11). Many putative risk factors have been identified as associated with an increased likelihood of an individual developing MS. These range from a strong association with the human leukocyte antigen (HLA)-DRB1 locus [a group of genes that serve as the major histocompatibility complex (MHC) (12)] to the identification of over 100 associated common variants that have been discovered with lower risk values (10). Some of these genetic loci are known to be involved in immunological activities, and have often been associated with other autoimmune disorders (9,10), but for many others any potential biological linkage to MS remains obscure (13,14).

We were particularly interested in findings that one of the genetic risk factors for MS maps to the locus for the lysosomal enzyme galactocerebrosidase (*GALC;* EC 3.2.1.46) (9,10,15), the gene that is responsible for causation of KD (6,16,17). KD is a devastating pediatric disorder that is associated with severe myelin damage, and may even be sometimes misdiagnosed as MS (18). In severe forms of KD, nervous system damage is so extensive as to typically cause death within 2-3 years after birth (19).

Based on the extensive myelin damage that occurs in KD, we hypothesized that the presence of a single mutant *GALC* allele might increase vulnerability of heterozygotes to myelin damage. What we found, however, was more unexpected and appears to offer a previously unrecognized alteration of biological functions relevant to tissue repair by a disease-relevant genetic risk factor. We found that *GALC* heterozygote (*GALC* +/−) mutant animals have apparently normal levels of myelin, oligodendrocytes and oligodendrocyte precursor cells and a similar degree of demyelination following 4 weeks of exposure to the well-studied myelinotoxic insult of cuprizone exposure. Where these mice were defective, however, was in remyelination and in the microglial phagocytic response that is necessary for the clearance of damaged myelin. Our results raise the possibility that common genetic variants identified through GWAS may contribute significantly to complex diseases, not by driving initial symptoms, but by altering repair mechanisms.

Results

WT and *GALC* +/− age-matched animals do not have any differences in myelin, oligodendrocytes, proliferating OPCs, or motor behavior

For many autosomal recessive disorders, individuals with one mutant allele and one WT allele are often considered unaffected. Although overt disease symptoms may not be present, we nonetheless first compared WT and *GALC* +/− animals to test for subtle neurological differences associated with heterozygous mutation of this gene. Due to the prevalent loss of myelin, oligodendrocytes, and proliferating oligodendrocyte progenitor cells (OPCs) in *twitcher* mice with two mutant *GALC* alleles (*GALC* −/−) ((20) and references therein) we were particularly interested in examining whether these populations were also affected in their heterozygous counterparts.

We did not observe any significant histological or behavioral differences between WT and *GALC* +/− animals at 3 months of age. We found no significant differences in corpus callosal myelin, as measured by FluoroMyelin (Invitrogen) staining (100.0 ± 4.53% for WT versus 94.63 ± 7.83% for *GALC* +/−; Fig. 1A; Supplementary Material, Fig. S1A), oligodendrocytes (Olig2/GSTπ) (100.0 ± 20.51% for WT versus 101.0 ± 5.42% for *GALC* +/−; Fig. 1B; Supplementary Material, Fig. S1B), or proliferating OPCs (Olig2/Ki67) (100.0 ± 4.98% for WT versus 100.1 ± 16.93% for *GALC* +/−; Fig. 1C; Supplementary Material, Fig. S1C). We also found no gross changes in motor function through analysis of several gait parameters (CleverSyS) that are altered in *GALC* −/− animals (20) (Fig. 1D).

GALC +/− mice also had normal levels of psychosine, the toxic lipid that accumulates in KD and that disrupts multiple lysosomal and cellular functions (see (20) and references therein) (0.006 ± 0.003 pmole psychosine per nmole phosphate for WT versus 0.001 ± 0.0002 pmole psychosine per nmole phosphate for *GALC* +/−).

GALC +/− animals have reduced remyelination following cuprizone exposure

The identity of relevant secondary insults remains largely unknown, but one possible candidate is tissue damage. Due to the myelin damage and failure of repair that occurs in both MS and KD (including in *GALC* −/−) mice (20–28), we examined whether heterozygous *GALC* +/− mice were more sensitive to a demyelinating insult and whether remyelination occurred normally following such an insult. To test this, we utilized the well-defined cuprizone model of demyelination (27,29,30). Cuprizone is a copper-chelating compound that causes oligodendrocyte toxicity, resulting in the loss of both oligodendrocytes and myelin in the corpus callosum after 4 weeks of feeding exposure (31). Upon removal of cuprizone, remyelination begins first with an increase in the recruitment and proliferation of OPCs, followed by differentiation of oligodendrocytes and finally the generation of new myelin, accompanied also by increases in neuroinflammation (30). As we previously observed significant loss of myelin, oligodendrocytes, and proliferating OPCs in the corpus callosum of *GALC* −/− *twitcher* mice (20), and changes in the corpus callosum are a prominent feature of MS (32), we were particularly interested to study whether there were increases in demyelination and/or deficits of remyelination in this region in the *GALC* +/− animals.

Two-month-old WT and *GALC* +/− littermates exposed to 0.3% cuprizone chow for 4 weeks were similar in the extent of

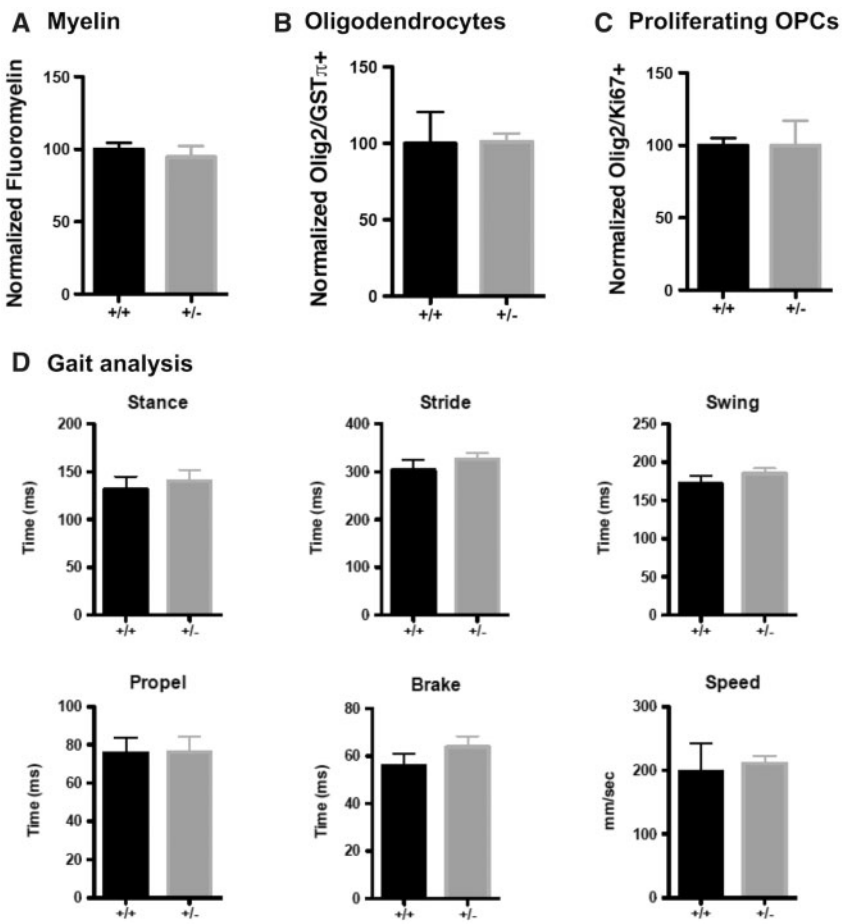

Figure 1. WT and *GALC* +/− age-matched animals do not have any differences in myelin, oligodendrocytes, proliferating OPCs, or motor behavior. (**A–C**) Quantification of (A) FluoroMyelin intensity, (B) the relative number of GSTpi+/Olig2+ oligodendrocytes, and (C) the relative number of dividing Ki67+/Olig2+ OPCs in the corpus callosa of three-month-old WT and *GALC* +/− littermates (N = 3 from different litters). Data are normalized to WT controls. (D) Quantification of stance, stride, swing, propel, and brake time, and travel speed, for three month old WT and *GALC* +/− littermates (N = 3 from different litters). Data for all graphs displayed as mean ± SEM.

corpus callosal myelin damage observed. All animals were monitored and weighed daily throughout cuprizone exposure to ensure that *GALC* +/− animals were not more sensitive to cuprizone toxicity. We did not observe a difference in weight loss during exposure or weight gain after removal from cuprizone chow, between WT and *GALC* +/− animals (Fig. 2A). Moreover, we observed similar reductions in myelin, as determined by FluoroMyelin labeling, in both WT and *GALC* +/− animals (0-wk: 11.47 ± 2.66% for WT versus 8.13 ± 1.57% for *GALC* +/−; Fig. 2B and C).

Where *GALC* +/− mice and their WT littermates did differ, however, was that at 2-weeks recovery, the *GALC* +/− animals had significantly less FluoroMyelin staining when compared to recovery-matched WT littermates (Fig. 2B and C). This reduction in FluoroMyelin staining persisted throughout the remaining weeks of recovery (2-wk $P < 0.01$: 68.29 ± 2.44% for WT versus 39.9 ± 4.16% for *GALC* +/−; 3-wk $P < 0.001$: 106.0 ± 6.13% for WT versus 56.48 ± 5.46% for *GALC* +/−; 4-wk $P < 0.05$: 92.93 ± 9.15% for WT versus 68.08 ± 6.18% for *GALC* +/−; Fig. 2B and C). Tissue examined by Western blot analysis also showed significantly less myelin oligodendrocyte glycoprotein (MOG; Supplementary Material, Fig. S2).

When we examined demyelination and remyelination at the cellular level, we again found that *GALC* +/− and WT mice were similarly sensitive to effects of cuprizone exposure but differed in their repair response. We observed a similar reduction in oligodendrocytes when we looked immediately following completion of cuprizone exposure (0-wk: 5.02 ± 0.20% for WT versus 5.26 ± 0.34% for *GALC* +/−; Fig. 2D). In contrast, we found significantly fewer oligodendrocytes during recovery in the *GALC* +/− animals when compared to recovery-matched WT littermates (3-wk $P < 0.001$: 74.79 ± 4.72% for WT versus 30.57 ± 1.90% for *GALC* +/−; 4-wk $P < 0.05$: 95.17 ± 2.29% for WT versus 73.21 ± 5.71% for *GALC* +/−; Fig. 2D). Thus, the decrease in oligodendrocytes observed later in recovery did not appear to be due to an increase in sensitivity of cells to cuprizone exposure.

Finally, when we quantified the pool of proliferating OPCs, the progenitor cell population critical to regenerating the lost oligodendrocytes necessary for subsequent remyelination, we also found a significant reduction in OPC number in the *GALC* +/− animals when compared to recovery-matched WT littermates (2-wk $P < 0.001$: 179.58 ± 18.44% for WT versus 95.74 ± 7.74% for *GALC* +/−; 3-wk $P < 0.001$: 194.58 ± 15.54% for WT versus 94.70 ± 16.2% for *GALC* +/−; Fig. 2E). In contrast, the initial proliferative OPC response to cuprizone injury was similar between WT and *GALC* +/− animals, indicating that *GALC* +/− OPCs likely do not have an intrinsic deficit preventing their proliferation, or a decrease early in recovery in OPC recruitment to the demyelinated areas (0-wk: 172.19 ± 6.93% for WT versus 145.93 ± 8.2% for *GALC* +/−; Fig. 2D).

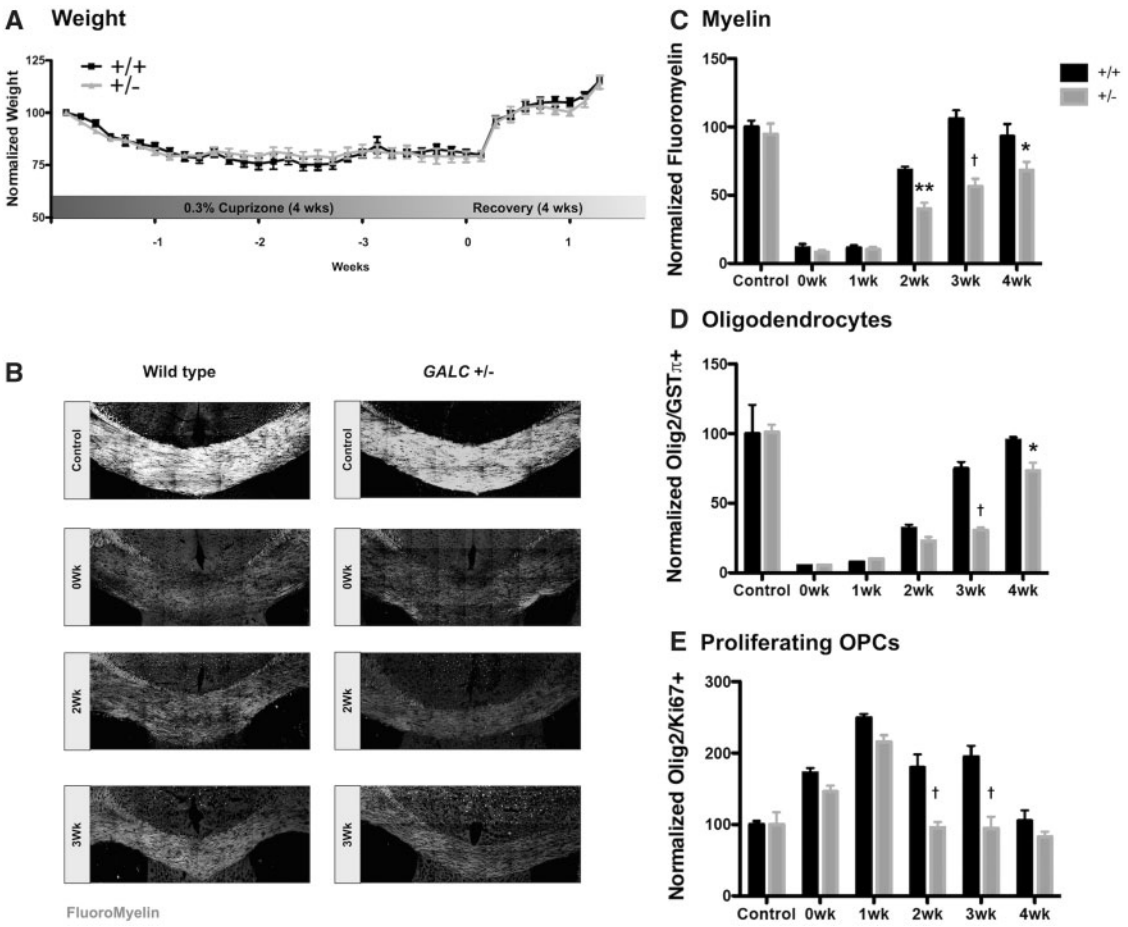

Figure 2. *GALC* +/− animals have reduced remyelination following cuprizone exposure. (**A**) Quantification of relative weights of WT and *GALC* +/− animals exposed to 0.3% cuprizone diet over the course of 4 weeks of exposure and 1 week recovery (N = 6 from different litters). (**B**) Representative confocal images of FluoroMyelin intensity. Quantification of (**C**) FluoroMyelin intensity, (**D**) number of GSTpi+/Olig2+ oligodendrocytes, and (**E**) the relative number of dividing Ki67+/Olig2+ OPCs in the corpus callosa of three-month-old WT and *GALC* +/− littermates after 4 weeks exposure to 0.3% cuprizone diet (N = 3 from different litters per time point). Data are normalized to WT untreated age-matched controls. Data for all graphs displayed as mean ± SEM. $^{*}P < 0.05$, $^{**}P < 0.01$, $^{\dagger}P < 0.001$ versus WT recovery-matched animals.

GALC +/− animals have elevated damaged myelin and altered microglial response following cuprizone exposure

As our experiments thus far suggested that the difference in myelin recovery between *GALC* +/− and WT mice was not due to different sensitivities to the induction of damage, we next examined the ability of cuprizone-treated mice to clear myelin debris, another critical component of the remyelination response. The clearance of myelin debris is necessary for repair following a demyelinating injury; delayed debris clearance can prevent proper OPC differentiation and subsequent remyelination (25,33,34). To determine if inefficient myelin debris clearance was contributing to the impaired remyelination we observed, we stained brains of treated mice with an antibody that specifically recognizes damaged Myelin Basic Protein [dMBP; (35,36)].

We found that, after 4 weeks of cuprizone exposure, both WT and *GALC* +/− animals had similar increases in dMBP staining (0-wk: 28.84 ± 0.47 fluorescent intensity [arbitrary units (a.u.)] for WT versus 25.55 ± 1.42 a.u. for *GALC* +/−; Fig. 3A and B). In contrast, no staining was observed in untreated, age-matched WT and *GALC* +/− animals.

When we examined the presence of myelin debris over the course of recovery, however, we found that *GALC* +/− animals had significantly more dMBP staining when compared to their WT counterparts at both 2- and 3-weeks of recovery (2-wk $P < 0.05$: 18.93 ± 2.07 a.u. for WT versus 29.09 ± 5.41 a.u. *GALC* +/−; 3-wk $P < 0.001$: 16.04 ± 1.46 a.u. for WT versus 29.37 ± 3.44 a.u. for *GALC* +/−; Fig. 3A and B). Thus, although the *GALC* +/− mice showed similar degrees of damage, the heterozygous carriers appeared to be deficient in clearing myelin debris throughout recovery.

Both monocytes and microglia have been implicated in the clearance of myelin debris necessary for efficient remyelination (22,30,37), however microglia appear to be the primary phagocytic cell responsible for contributing to remyelination after cuprizone injury [e.g. (27,29,30,34)]. Additionally, microglia have been shown to express the *GALC* gene (38), although it's functional relevance within these cells is unknown. Because of the role of microglia in myelin debris clearance, as well as the increase in damaged myelin observed in the *GALC* +/− animals, we analyzed this population further.

We found that, immediately following cuprizone exposure, both WT and *GALC* +/− animals appeared to have mounted a similar microglial response. We first examined the presence and morphology of microglia in the corpus callosa of cuprizone-injured animals through staining with Iba-1, a microglia specific marker (39). WT and *GALC* +/− mice had a similar increase in

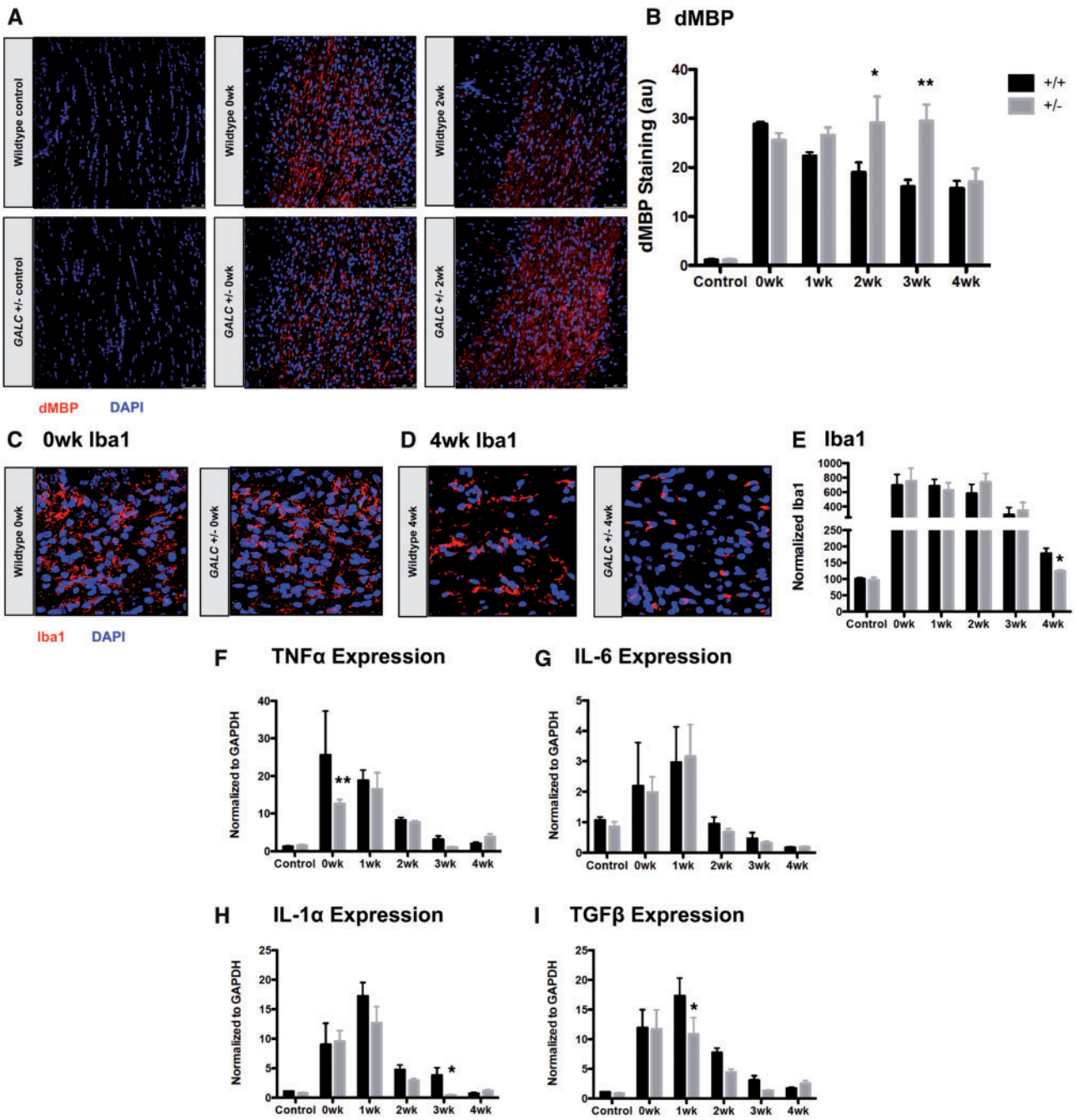

Figure 3. *GALC* +/− animals have elevated damaged myelin and altered microglial response following cuprizone exposure. (**A,B**) Representative confocal images and quantification of damaged Myelin Basic Protein (dMBP) in the corpus callosa of three-month-old WT and *GALC* +/− littermates after 4 weeks exposure to 0.3% cuprizone diet (N = 3 from different litters per time point). (**C–E**) Representative confocal images and quantification of Iba-1 microglial staining in (C) 0-week cuprizone recovery WT and *GALC* +/− animals, (D) 4-week cuprizone recovery WT and *GALC* +/− animals, and (E) quantification of Iba-1 staining in the corpus callosa of three month old WT and *GALC* +/− littermates after 4 weeks exposure to 0.3% cuprizone diet (N = 3 from different litters per time point). Data are normalized to WT controls. (**F–I**) Quantification of the relative levels of mRNA of (F) tumor necrosis factor alpha (TNFα), (G) interleukin-6 (IL-6), (H) interleukin-1 alpha (IL-1α), and (I) transforming growth factor beta (TGFβ). Data are normalized to GAPDH and represented as fold change over WT untreated controls (N = 3 from different litters). Data for all graphs displayed as mean ± SEM. $^{*}P < 0.05$, $^{**}P < 0.01$ versus WT recovery-matched animals.

Iba-1 microglial staining (0-wk: 693.21 ± 153.11% for WT versus 751.23 ± 183.05% for *GALC* +/−; Fig. 3C and E). The morphology of microglia at this time also appeared similar.

Tissue examined at 4 weeks recovery revealed a somewhat more rapid return to baseline for numbers of microglia in the corpus callosa of heterozygote mutant mice, as detected by Iba-1 microglial staining in the *GALC* +/− animals when compared to recovery-matched WT animals (4-wk $P < 0.05$: 178.93 ± 15.87% for WT versus 124.37 ± 4.2% for *GALC* +/−; Fig. 3D and E). We observed a more striking difference, however, in the morphology of the microglia between the WT and *GALC* +/− animals at 4-weeks recovery. The WT microglia appeared more ramified, with increased process complexity, while the *GALC* +/− microglia appeared to have stunted, less complex processes (Fig. 3D).

To further characterize the microglial response in cuprizone-injured animals, we next analyzed expression of several cytokines known to be elevated following cuprizone exposure, including TNFα, IL-6, IL-1α, and TGFβ (40,41) (Fig. 3F–I). Although we did find some differences in expression at isolated recovery time points between WT and *GALC* +/− animals (TNFα at 0-wk: 25.6 ± 11.72-fold for WT versus 12.57 ± 1.17-fold for *GALC* +/− $P < 0.01$; IL-1α at 3-wk: 3.83 ±1.27-fold for WT versus 0.384 ± 0.13-fold for *GALC* +/− $P < 0.05$; and TGFβ at 1-wk: 17.31 ± 3.08-fold for WT versus 10.84 ± 2.81-fold for *GALC* +/− $P < 0.05$; Fig. 3F, H and I, respectively), we generally saw similar increases in expression early in recovery (0-, 1-week) that declined at later recovery time points (Fig. 3F–I).

Taken together, *GALC* +/− microglia had a similar pro-inflammatory response early in recovery following cuprizone-induced demyelination to WT, but showed some evidence of an altered response as recovery progressed. Although an increased inflammatory response could be a theoretical contributor to defective repair processes, our studies do not suggest the existence of such an increase.

GALC +/− microglia have impaired myelin phagocytosis

In addition to the expression of pro-inflammatory cytokines and infiltration into the corpus callosum, microglia also play a critical role in tissue repair following a demyelinating insult through the phagocytic clearance of myelin debris (22,30,34,37,41). Due to the elevated levels of damaged myelin present in the corpus callosa of *GALC* +/− animals, we next tested whether *GALC* +/− animals had reduced myelin phagocytosis by analyzing the number of microglia co-localized with myelin (Iba-1/FluoroMyelin, Fig. 4A; Supplementary Material, Fig. S3A). The density of microglia in the corpus callosa of animals at 0- and 1-week recovery time points was too great to accurately count individual cells, so we focused our efforts on analyzing the 2- and 3-week recovery time points, when we began seeing decreases in remyelination (Fig. 2B and C).

We found significantly fewer Iba-1/FluoroMyelin double-positive microglia at 2- and 3-weeks post-cuprizone treatment in the *GALC* +/− animals compared to WT (2-wk $P < 0.01$: 25.47 ± 2.49 cells/field for WT versus 17.73 ± 0.5 cells/field for *GALC* +/−; 3-wk $P < 0.05$: 10.77 ± 0.52 cells/field for WT versus 5.17 ± 0.71 cells/field for *GALC* +/−; Fig. 4A). These results suggested the *GALC* +/− microglia were less effective at myelin phagocytosis compared to WT.

We also found that microglia from *GALC* +/− mice had decreased expression of Triggering receptor expressed on myeloid cells-2, or Trem2, which is thought to play an important role in microglial clearance of myelin debris (42). Elevated expression of Trem2 has been used as a readout of myelin phagocytosis after cuprizone exposure (34,43). Interestingly, loss of Trem2 function leads to impaired remyelination following cuprizone-induced demyelination (43), a phenotype strikingly similar to what we observed in our *GALC* +/− animals.

When we examined the expression of Trem2 in cuprizone-injured animals, we found that there was a significant reduction in expression in *GALC* +/− animals when compared to WT recovery-matched animals at the same time points where reductions in Iba1/FluoroMyelin positive microglia were also observed (2-wk $P < 0.05$: 19.75 ± 2.18-fold for WT versus 8.92 ± 0.882-fold for *GALC* +/−; 3-wk $P < 0.001$: 33.36 ± 8.35-fold for WT versus 4.82 ± 1.32-fold for *GALC* +/−; Fig. 4B). Additionally, we found a significant reduction in expression of alphaM/beta2 integrin complement receptor-3 (MAC-1/CR3), another microglial receptor involved in myelin debris phagocytosis (44), at 2-weeks of recovery ($P < 0.05$: 10.79 ± 3.5-fold for WT versus 2.19 ± 0.39-fold for *GALC* +/−; Supplementary Material, Fig. S3B). Taken together, these data suggested that although *GALC* +/− microglia had similar numbers and morphology to WT mice immediately following cuprizone exposure, these cells had an altered response to myelin damage during the repair processes carried out after cuprizone exposure was stopped.

To directly test whether *GALC* +/− microglia had impaired myelin phagocytosis, we performed a myelin phagocytosis assay *in vitro*. Both microglia and myelin debris were isolated from the brains of 3-month-old WT and *GALC* +/− littermates [$n = 3$ animals per genotype; (45)]. Isolated microglia were confirmed through positive staining with Iba-1 (Supplementary Material, Fig. S3C). Isolation of microglia from the whole brain provided a population of cells in which the contribution of corpus callosal microglia would have been relatively small. Thus, it is likely that any functional differences observed in these assays are indicative of functional alterations that are not restricted to cells of the corpus callosum. Additionally, myelin debris was analyzed to ensure proper isolation, and was found to contain several myelin proteins, including myelin-associated glycoprotein (MAG; ∼63 kDa), myelin oligodendrocyte glycoprotein (MOG; ∼27 kDa), and myelin basic protein (MBP; 21, 18, 17, and 14 kDa) (Supplementary Material, Fig. S3D).

To test the phagocytosis of myelin debris by microglia, we labeled isolated myelin with the lipophillic dye Di-I (Invitrogen) and treated the cells overnight with 20μg of labeled myelin debris. Cells were then washed to remove excess debris, stained with Hoechst, and imaged on a laser confocal (Leica) to quantify the amount of phagocytosed myelin. To ensure that myelin engulfment was occurring through phagocytic-mediated endocytosis, we used Dynasore (Dyn; Sigma), a dynamin inhibitor that blocks endocytosis (46,47).

We found that, in *GALC* +/− microglia, there was significantly less myelin engulfed by the cells compared to WT microglia (13.02 ± 1.92 a.u. for WT unt versus 6.22 ± 0.68 a.u. for *GALC* +/− unt $P < 0.01$; Fig. 4C; Supplementary Material, Fig. S3E). Treatment with Dyn markedly reduced myelin debris engulfment by the microglia from both WT and *GALC* +/− animals (13.02 ± 1.92 a.u. for WT unt versus 2.07 ± 0.62 a.u. for WT Dyn $P < 0.01$; 6.22 ± 0.68 a.u. for *GALC* +/− unt versus 1.34 ± 0.56 a.u. for *GALC* +/− Dyn $P < 0.05$; Fig. 4C; Supplementary Material, Fig. S3E). Such results further indicated the differences seen between WT and *GALC* +/− microglia were due to myelin engulfment.

Our *in vitro* studies also demonstrated that *GALC* +/− microglia exhibited a compromised ability to elevate Trem2 when challenged with myelin debris. Exposure of WT microglia to myelin debris caused a nearly six-fold increase in Trem2 expression, consistent with their effective myelin phagocytosis (1.16 ± 0.42-fold for WT unt versus 5.79 ± 2.15-fold for WT + myelin $P < 0.01$; Fig. 4D). In contrast, *in vitro* exposure to myelin debris did not trigger an increase in Trem-2 expression in microglia isolated from *GALC* +/− animals, again consistent with the reduced myelin phagocytosis observed in these cells (0.64 ± 0.26-fold for *GALC* +/− unt versus 0.69 ± 0.21-fold for *GALC* +/− + myelin; Fig. 4D).

Our studies on *GALC* −/− mice had shown that the increasingly alkalized lysosomal pH that occurs in OPCs of these animals caused reductions in endocytic transport and impaired lysosomal function (20). Such pH differences did not seem to contribute to defective myelin engulfment in microglia isolated from *GALC* +/− mice, however, as we found no significant

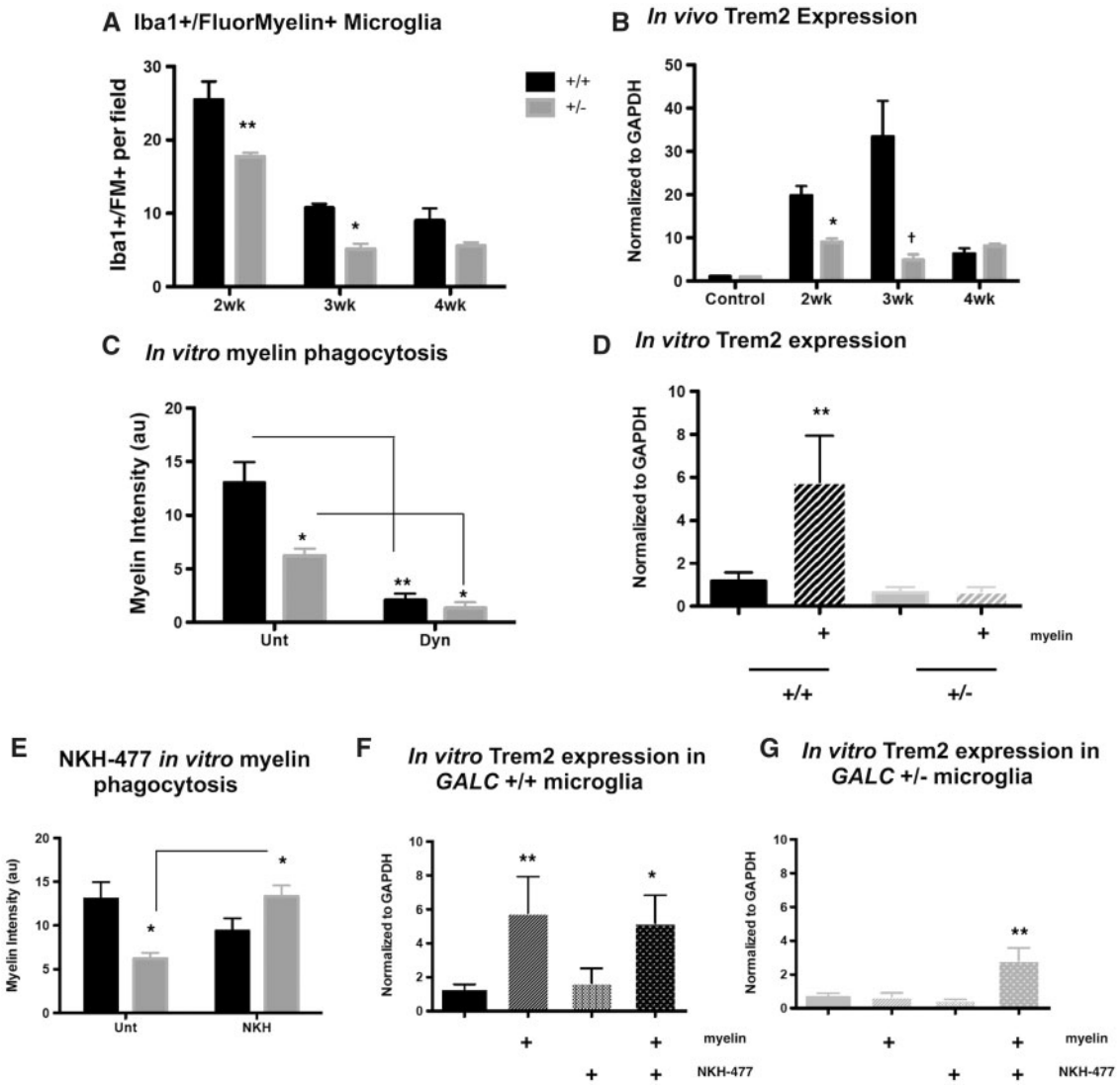

Figure 4. *GALC* +/− microglia have reduced myelin phagocytosis *in vivo* following cuprizone exposure and *in vitro*. (**A**) Quantification of Iba-1 and FluoroMyelin staining in the corpus callosa of three month old WT and *GALC*+/− littermates after 4 weeks exposure to 0.3% cuprizone diet (N = 3 from different litters per time point). Data are represented as the average number of Iba-1+/FluoroMyelin+ cells per field of view. (**B**) Quantification of the relative levels of mRNA of Triggering receptor on myeloid cells 2 (Trem2). Data are normalized to GAPDH and represented as fold change over WT untreated controls (N = 3 from different litters). (**C**) Quantification of myelin phagocytosis: isolated microglia from three-month-old WT and *GALC* +/− littermates were loaded with Di-I (Invitrogen) labeled myelin overnight and imaged (N = 3 from different litters). Myelin phagocytosis was quantified by measuring fluorescent intensity. Cells were pretreated with Dynasore (100μM; Sigma) 1 h prior to myelin debris loading as a control. (**D**) Quantification of the relative levels of mRNA of Trem2 in isolated WT and *GALC* +/− microglia either untreated or treated overnight with myelin debris. Data are normalized to GAPDH and represented as fold change over WT untreated controls (N = 3 from different litters). (**E**) Quantification of myelin phagocytosis as described in (**C**); cells were left either untreated or treated with NKH-477 (1μM; Tocris) upon myelin loading. (**F,G**) Quantification of the relative levels of mRNA of Trem2 in isolated WT (**F**) and *GALC* +/− (**G**) microglia either untreated or treated overnight with myelin debris, with or without the addition of NKH-477 (1μM). Data are normalized to GAPDH and represented as fold change over WT untreated controls (N = 3 from different litters). Data for all graphs displayed as mean ± SEM. *P < 0.05, **P < 0.01, †P < 0.001 versus WT recovery-matched animals; *P < 0.05, **P < 0.01 versus WT untreated microglia.

differences in lysosomal pH between WT or *GALC* +/− microglia (4.41 ± 0.11 for WT versus 4.19 ± 0.33 for *GALC* +/−; Supplementary Material, Fig. S3F).

The ability to study myelin debris uptake *in vitro* also enabled us to ask whether therapeutic approaches developed in our studies on KD and other sphingolipidoses (20) might be of potential value in improving debris uptake in *GALC* +/− cells. In our previous studies, we found that exposure to psychosine disrupts multiple lysosomal and cellular functions and that we were able to protect against these disruptions *in vitro* and *in vivo* with drugs that converge on restoring normal regulation of lysosomal function. One of these drugs, NKH-477 (also known as colforsin), was of particular interest due to its efficacy *in vivo* in *GALC* −/− (*twitcher*) mice and its ability to also restore normal endolysosomal trafficking *in vitro* (20).

When we treated WT and *GALC* +/− microglia with NKH-477 (1 μM) we found that, in WT microglia, NKH-477 did not significantly affect myelin phagocytosis (13.02 ± 1.92 a.u. for WT unt versus 9.35 ± 1.45 a.u. for WT + NKH-477; Fig. 4E; Supplementary Material, Fig. S3G) or expression of Trem2 (1.16 ± 0.42 a.u. for WT unt versus 1.65 ± 0.86 a.u. for WT + NKH-477 versus 5.19 ±1.64 a.u. for WT + NKH + myelin; Fig. 4F). However, myelin phagocytosis was significantly improved in *GALC* +/− microglia treated with NKH-477 (6.22 ± 0.68 a.u. for *GALC* +/− unt versus

13.32 ± 1.25 a.u. for *GALC* +/− +NKH $P < 0.05$; Fig. 4E; Supplementary Material, Fig. S3F) to levels similar to WT cells. NKH-477 treatment also significantly elevated Trem2 expression in GALC +/− microglia exposed to myelin debris (0.64 ± 0.26 a.u. for *GALC* +/− unt versus 0.48 ± 0.04 a.u. for *GALC* +/− + NKH-477 versus 2.82 ± 0.76 a.u. for *GALC* +/− + NKH-477 + myelin; Fig. 4G).

Discussion

Our studies on the biological consequences of expression of a single mutated *GALC* gene, a risk factor for the development of MS, have revealed that this genetic alteration compromises the repair of demyelinating damage in the CNS and causes inefficient myelin debris clearance by microglia. Under basal homeostatic conditions we did not find any differences between WT and *GALC* +/− animals, nor did we find any differences in the extent of damage caused by four weeks of cuprizone exposure, indicating a similar vulnerability to this insult. During the period of repair, however, *GALC* +/− animals had significantly reduced remyelination, along with lower numbers of oligodendrocytes and proliferating OPCs. We further found elevated levels of damaged myelin in the corpus callosa of *GALC* +/− animals during the recovery period, along with reductions in microglia co-localized with myelin puncta and reductions in the expression of the microglial protein Trem2. Direct testing of myelin phagocytosis in isolated microglia showed that *GALC* +/− microglia had significantly reduced myelin phagocytosis as compared to cells isolated from WT animals and confirmed a decreased ability to upregulate Trem2 in response to exposure to myelin debris. Finally, treatment with NKH-477 a forskolin derivative that we discovered is able to enhance lysosomal function (20), improved myelin phagocytosis in *GALC* +/− microglia and also elevated levels of Trem2 expression.

The mathematical identification of genetic loci that increase the risk for a large variety of diseases has greatly outpaced the understanding of the biological functions that are altered by the presence of such risk factors. For example, over 100 variants have been identified as increasing the risk for the development of MS (10). Many of these variants are thought to influence immunological function, but documented changes in biological function that might be relevant to MS are largely unknown.

GALC mutations provide an interesting example of the above dilemma. *GALC* was one of the strongest vulnerability loci identified in the GWAS study conducted by the International Multiple Sclerosis Genetics Consortium and the Wellcome Trust Case Control Consortium (9,10). This was one of the few loci in this study to show an odds ratio >1.2 and an allele frequency close to 1, and more recent studies have identified intronic variants of *GALC* predicted to lead to splice-region variants as one of the 110 strongest risk factors associated with MS (10). While it remains unknown if the variants identified by the MS GWAS are associated with Krabbe disease, intronic variants have been described in several late-onset KD patients (48), and variants leading to altered mRNA splicing are also known to cause disease (49). The results of our present study indicate, however, that changes in *GALC* can cause biological changes of potential relevance to MS. Moreover, the predicted frequency in the population of *GALC* mutations capable of causing KD when both alleles are mutated is approximately 1:125-150 (6), a large enough fraction of the population to offer a viable candidate for disease-relevance.

Possible relevance of our finding to MS and other neurological diseases

Impaired myelin debris clearance is thought to contribute to the inefficient remyelination that is often observed in MS patients, particularly in patients with progressive MS where the imbalance of demyelination and remyelination leads to severe neurological disability (21–26,50). The presence of damaged myelin also can prevent the differentiation of OPCs into oligodendrocytes, impairing proper remyelination and ultimately leading to degeneration (33). Moreover, it is thought that the inability to efficiently repair demyelinated lesions is what ultimately leads to the development of progressive MS (21–26,50). Microglia, the CNS-resident immune cells, are thought to be important in multiple aspects of MS pathology (22,26,30,34,37). They contribute to the neuroinflammation that can cause widespread tissue damage, and also play critical roles in normal neural development, tissue surveillance and repair, and debris clearance necessary for repair (22,26,30,31,34,37,41,50–53).

The decreases in myelin debris clearance caused by carrying a *GALC* mutation thus offer an alteration in biological function that is attractive for its potential relevance to MS. It was particularly interesting that decreased clearance of myelin debris in the CNS of *GALC* +/− mice only became apparent as recovery was progressing. One possible interpretation of our observations is that *GALC* +/− microglia may be hypersensitive to overload, resulting in lower thresholds of myelin debris that can be efficiently phagocytosed and eliminated. It recently was shown that microglia can become overburdened when processing myelin debris, resulting in lysosomal inclusions and neuroimmunological dysfunction (47). Why this defect was not apparent in our studies during the period of cuprizone treatment itself is not known, but it may be that cuprizone modifies microglial function such that other aspects of function of these cells are dominant during the actual time of treatment. It appears that *GALC* +/− microglia may be hypersensitive to myelin debris overload, resulting in lower thresholds of myelin debris that can be efficiently phagocytosed and eliminated.

Our results are also intriguing in appearing to offer the first example of a case in which heterozygous status for a mutation that causes a recessive disease is sufficient to decrease the efficiency of tissue repair. The idea that being a heterozygous carrier for such a mutation might increase susceptibility to damage, or the likelihood of such damage occurring, would be consistent with current interpretations of findings that being a heterozygous carrier for mutations that cause Gaucher disease increase the likelihood of development of Parkinson's disease (3–5). Disease pathogenesis has many components, however, and a failure to repair damage effectively would mean that lesions that might be relatively harmless after repair could now have the opportunity to become more serious. In future studies, it will be interesting to determine whether such disruption of repair is peculiar to mutations in the GALC gene or whether it is also associated with, for example, carrier status for mutations causing other lysosomal storage disorders.

While we can find no prior information that predicts any association of *GALC* with Trem2 function, this finding seems to have potential relevance that will deserve exploration in future studies. For example, in the context of why changes in *GALC* might be associated with an increased risk of MS, engagement of Trem2 decreases inflammation, and blockade of Trem2 worsens disease progress in the experimental allergic encephalomyelitis (EAE) animal model of MS (54). Conversely, transplantation of myeloid precursor cells genetically modified

to express Trem2 limits tissue destruction in this same model (55). Trem2 appears to be critical for the response to demyelination (42), and loss of Trem2 function leads to impaired remyelination following cuprizone-induced demyelination, much like the phenotype we observed in *GALC* +/− mice. In humans, loss-of-function mutations in Trem2 cause the rare Nasu-Hakola disease, which is associated with demyelination of subcortical white matter damage and lethal early onset dementia (56).

Defects in Trem2 function also may have implications that extend beyond illnesses with myelin damage as a critical contribution to disease pathology. For example, in respect to microglial function, Trem2 is also critical for clearance of neuronal apoptosis (57) and of amyloid plaques in the presence of anti-amyloid beta antibodies (58). Alterations in Trem2 function are of active interest in respect to Alzheimer's disease and potentially other neurodegenerative disorders (42,59–69). Trem2 knockdown also worsens outcomes in experimental stroke models (70) and Trem2 loss may even generally accelerate aging processes (42,71).

The changes in microglial function in GALC +/− mice also extend beyond disrupting regulation of Trem2 expression. We also saw a significant reduction in expression of MAC-1/CR3, another microglial receptor involved in myelin debris phagocytosis (44). In addition, the changes in microglial morphology that are associated with activation of these cells were altered in microglia of the GALC +/− mice during the period of myelin repair. As our *in vitro* studies were conducted on microglia isolated from the whole brain, it seems unlikely that the changes seen in examination of the corpus callosum *in vivo* pertain only to microglia in this single CNS region. Collectively, these observations provide a foundation for future studies targeted at understanding how heterozygosity for a mutant allele at the GALC locus alters microglial function.

The identification of microglial dysfunction was complemented by the demonstration that NKH-477, a pharmacological agent identified in our studies on lysosomal storage disorders (20), was able to restore normal myelin debris uptake and increase levels of Trem2 expression in GALC +/− microglia *in vitro*. We previously discovered that different toxic lipids that accumulate in Krabbe disease, Gaucher disease, metachromatic leukodystrophy and Fabry disease all appear to disrupt lysosomal function by causing lysosomes to become abnormally alkaline. Drug repurposing studies led to the identification of several structurally diverse compounds that prevented multiple lysosomal and cellular toxicities caused by these lipids, and did so by promoting lysosomal re-acidification. NKH-477, one of these compounds, was examined *in vivo* because it is CNS penetrant, and we found that daily treatment of *twitcher* (GALC−/−) mice with this drug protected against myelin damage and loss of oligodendrocyte lineage cells, and also extended lifespan as effectively as gene therapy. As NKH-477 is a forskolin derivative that increases cAMP levels, it likely has multiple effects on cellular function. Nonetheless, it will be of interest in future studies to determine whether the defects in microglial function we observed in GAL+/− cells are caused by lysosomal dysfunction, whether the benefits of NKH-477 treatment can be obtained by other agents that promote lysosomal re-acidification and whether any such drugs restore normal remyelination in vivo in GALC +/− mice.

The ability of changes in *GALC* to impair microglial function might also be relevant to other disease risks associated with being a heterozygous carrier of disease-relevant mutations in this enzyme. Heterozygous carriers of mutations of *GALC* may be at increased risk for open angle glaucoma (2), another disease in which compromised damage repair could contribute to disease pathogenesis. The *GALC* locus also was recently reported as a risk factor for pulmonary artery enlargement in association with chronic obstructive pulmonary disease (72), another condition in which proper function of myeloid cells is relevant, and also has been suggested to be of possible relevance in late-onset synucleinopathies (73).

If the above considerations were correct, then it would be of particular interest to more comprehensively identify diseases for which *GALC* heterozygosity is a risk factor. Identification of the linkage between *GALC* and other diseases has thus far been based on the unbiased detection of such linkage in studies focused on a particular disease entity [as in, e.g. MS (9,10), glaucoma (2), pulmonary artery enlargement (72) or synucleinopathies (73)]. Going forward, however, it may be more efficient to obtain detailed family histories from parents of children with KD; as such parents are obligate heterozygous carriers of disease-causing mutations. Such analyses may reveal much more rapidly a spectrum of disorders for which changes in GALC function need to be considered. In addition, it may be of future interest to directly determine the prevalence of *GALC* mutations in MS patients, as a prelude to considering whether individuals with such mutations could benefit from treatments aimed at improving *GALC* enzymatic activity in Krabbe disease patients (20,74–76).

Materials and Methods

Ethics statement

The University of Rochester RSRB has reviewed this study and determined that based on federal (45 CFR 46.102) and University criteria the study does not qualify as human subjects research and has waived the need for consent (RSRB#00024759). All animal procedures were performed under the guidelines of the National Institutes of Health and approved by the Institutional Animal Care and Utilization Committee (IACUC) of the University of Rochester Medical Center, Rochester, NY (UCAR#2001-140).

Animal treatment

Adult heterozygote (*GALC* +/−) C57Bl/6J (B6.CE-Galctwi/J) mice were originally obtained from Dr. Ernesto Bongarzone (University of Illinois at Chicago, Chicago, IL) and used as breeder pairs to generate heterozygote (*GALC* +/−) and wild-type (WT; *GALC* +/+) C57Bl/6J mice. All animal procedures were approved by the Institutional Animal Care and Use Committee (IACUC) at the University of Rochester School of Medicine and Dentistry and conformed to the requirements of the Animal Welfare Act. Three-month old untreated WT ($n = 3$) and *GALC* +/− ($n = 3$) mice were utilized as controls. In total, two cohorts of aged-matched mice from different litters were fed chow with 0.3% cuprizone [(Bis(cyclohexanone)oxaldihydrazone; Sigma #45-14690; (31)] for 4 weeks and weighed daily: WT mice ($n = 30$); *GALC* +/− mice ($n = 30$). Mice were euthanized every week following exposure (0–4 weeks; $n = 6$ from each cohort). For immunohistochemical analysis (described below) tissue from WT ($n = 3$) and *GALC* +/− ($n = 3$) animals was isolated following transcardial perfusion with 4% paraformaldehyde. For quantitative PCR (qPCR) analysis (described below), tissue from WT ($n = 3$) and *GALC* +/− ($n = 3$) animals was isolated following transcardial perfusion with ice-cold PBS.

Immunohistochemistry

Mice were transcardially perfused with 4% paraformaldehyde/PBS. Isolated tissue was post-fixed for 24h in 4%

paraformaldehyde, and normalized for 48 h in 20% sucrose. Brains were sectioned at 15μm thickness in OCT (Tissue Tek) using a cryotome (Leica) and immunostained with Ki67 (1:250; BD Pharmingen #550609), Olig2 (1:500; Millipore #MABN50), GST0 (1:500; BD Biosciences #610718), FluoroMyelin (Invitrogen), damaged MBP (dMBP; 1:1000; Millipore #AB5864), Iba-1 (1:1000; Fisher Scientific #019-19741) and DAPI (Invitrogen). Mosaic images were acquired using a Leica TCS SP5 laser confocal microscope with a 40x oil immersion lens. Data represent analyses of the corpus callosa (CC) of at least 3 WT and *GALC* +/− brains from separate litters.

Motor behavior testing

Three-month old WT ($n = 3$) and *GALC* +/− ($n = 3$) mice from different litters were analyzed for locomotive ability and gait using the Phenoscan suite and Runwayscan software (CleverSys, Inc). Multiple parameters, including stance, stride, swing, brake, and propulsion time (milliseconds), stride length (millimeters), and average speed (millimeters/second) were collected for each animal over 3 compliant trials and averaged for both front and rear paws.

Quantitative PCR (qPCR)

Mice were transcardially perfused with ice-cold PBS. RNA was isolated from corpus callosal tissue using a Nucleospin RNA isolation kit (Fisher Scientific) as per manufacturer's directions and converted to cDNA using iScript cDNA synthesis kit (Bio-Rad). All TaqMan probe assays were purchased through ThermoFisher: interleukin-1 alpha (IL-1α; Mm00439620_m1), interleukin-6 (IL-6; Mm00446190_m1), tumor necrosis factor alpha (TNFα; Mm00443258_m1), transforming growth factor beta (TGFβ; Mm01178820_m1), Trem2 (Mm04209424_g1), and Itgam (Mac1/CR3; Mm00434455_m1). Assays were run using SsoAdvanced Universal Probes Super Mix (Bio-Rad) in 364-well plates on a Bio-Rad C1000 Thermal Cycler and multi-plexed with GAPDH (Applied Biosystems; #1207039). All plates included untreated WT and *GALC* +/− age-matched controls for normalization. Three different animal samples were run in triplicate for each probe.

Microglia isolation and culture

Microglia were isolated following the protocol from Lee *et al.* (45). Briefly, 3 month-old WT ($n = 3$) and *GALC* +/− ($n = 3$) animals were transcardially perfused with ice-cold PBS, the brains were removed, finely minced with a sterile blade, and enzymatically digested for 20 min in dissociation media (Dispase (Roche), Dnase (Invitrogen), Papain (Sigma) solution). Dissociated cells were strained through a 40μM cell strainer and separated using a Percoll (Sigma) gradient. Isolated cells were then seeded on glass-bottom microwell dishes (MatTek Co., Ashland, MA; #P35G-1.5-14) in DMEM/F12 supplemented with Pen/Strep (1:100; Sigma), glucose (4500 mg/l), and heat-inactivated FBS (inactivated for >30 min at 56 °C). Microglia were maintained for 7d at 37 °C (7% CO_2) before initiation of experiments, with a 50% media change every third day.

Myelin isolation, labeling, and phagocytosis analysis

Myelin debris was isolated from the Percoll gradient described above, rinsed in PBS, quantified for protein content using standard methodology (BCA Protein Assay, Pierce), and stored at -80 °C until use. To ensure proper isolation, myelin debris from each sample was analyzed via Western blot for several myelin related proteins (described below). To perform the myelin phagocytosis assay, twenty micrograms of myelin debris from each sample was labeled with the lipophilic dye Di-I (1:200; Invitrogen) and incubated at 37 °C following manufacturer's instructions. Labeled myelin debris was then added to fresh microglia culture media, and incubated with cells overnight. Following incubation, all media were removed and replaced with fresh culture media. Cells were then labeled with Hoechst (1:1000; Invitrogen) and imaged using a Leica TCS SP5 laser confocal microscope with a 63X oil immersion lens. Phagocytosed myelin was quantified using Leica software and averaged for each animal. To ensure that myelin engulfment was occurring through phagocytic-mediated endocytosis, we pretreated cells with Dynasore (100ore (100t myeldynamin inhibitor that blocks endocytosis (46,47) 1 h prior to myelin debris loading. NKH-477 (1μM; Tocris) was added to microglia during myelin debris loading, and analyzed 24 h later.

Immunoblotting

Twenty micrograms of each sample was electrophoretically separated using 4-12% gradient Novex© PAGE gels as per manufacturer's instructions (XCell SureLockTM Mini-Cell Electrophoresis System, Invitrogen). Electrophoresed proteins were transferred to PVDF membranes (Immobilon©-P, Millipore) using a Mini Trans-Blot© transfer system (Bio-Rad), as per manufacturer's instructions. After transfer, PVDF membranes were blocked for 1h with gentle rocking in 1X TBS-T with 3% BSA Fraction V (Sigma #A3059) before overnight incubation with primary antibodies [myelin-associated glycoprotein (MAG; 1:1000 Millipore #MAB1567), myelin oligodendrocyte glycoprotein (MOG; 1:1000 ThermoFisher #MAB5680MI), and myelin basic protein (MBP; 1:1000 ThermoFisher #MAB3841MLMI)] in 1X TBS-T with 3% BSA. Following TBS-T washes and incubation with HRP-conjugated secondary antibodies (in 1X TBS-T with 1% BSA), PVDF membranes were incubated with ECL reagent (Amersham ECL Prime, GE Life Sciences) and HRP signal was detected on autoradiography film (Amersham Hyperfilm, GE Live Sciences). PVDF membranes were de-probed and re-probed using standard denaturing/reducing methods. The following HRP-conjugated secondary antibodies were from Santa Cruz Biotechnology: goat-anti-mouse IgG (#sc-2005), goat-anti-mouse IgG1 (#sc-2060), goat-anti-mouse IgG2a (#sc-2061), goat-anti-mouse IgG2b (#sc-2062). Band optical density was quantified using ImageJ.

Immunocytochemistry

Isolated microglia were fixed with 4% paraformaldehyde for 20 min prior to permeabilization for 10 min with 0.5% Triton X-100 (Sigma #X100) in blocking media (Earl's Balanced Salt Solution (Gibco) with 5% calf serum and 1% BSA Fraction V). Permeabilized cells were then blocked for 1h at 25 °C before overnight incubation with Iba-1 (1:1000; Fisher Scientific #019-19741) diluted in blocking media at 4 °C. After washing, cells were incubated with species- and isotype-matched Alexa Fluor-conjugated secondary antibodies (1:2000; Invitrogen) and counterstained with DAPI (1μg/ml; Invitrogen #D1306) for 30 min at 25 °C before final washes with PBS and ddH_2O.

Lysosomal pH measurements

Isolated microglia were plated on glass-bottom microwell dishes. Cells were loaded with 500μg/ml Lysosensor Yellow/Blue Dextran (Invtirogen) for 24 h then imaged using a Leica TCS SP5 laser confocal microscope with a 63X oil immersion lens. Using an excitation wavelength of 335 nm (405 diode), emission spectra at 450 nm (acidic) and 521 nm (alkaline) were quantified, and the ratio of these emissions was calculated using the Leica Advanced Fluorescence software. To generate the lysosomal pH calibration curve, the pH of pre-loaded microglia was measured as previously described (20,77). Briefly, the cells were incubated in calibration buffers (20 mM MES, 110 mM KCl, and 20 mM NaCl containing 10μM monensin and 20μM nigericin; Sigma), adjusted to known pH values between 4.0 and 6.0 at 0.5 increments using HCl/NaOH for 1h prior to imaging, and ratiometric quantification was performed, as described above.

Psychosine quantification

Mice were euthanized at P35 and transcardially perfused with ice-cold PBS. Isolated tissue was flash-frozen in liquid nitrogen and stored at -80 °C until analysis. Analysis of psychosine was performed by Dr. Jacek Bielawski from the Lipidomics Core at the Medical University of South Carolina (MUSC) using liquid chromatography-mass spectrometry (LC-MS/MS) and supercritical fluid chromatography- mass spectrometry (SFC-MS/MS) methodologies as described previously (78).

Statistical analyses

Bar graphs are plotted as mean ± SEM and represent at minimum three independent biological replicates performed in triplicate, except where noted. Two-group comparisons were analyzed using a Student's T-test and multiple-group comparisons were analyzed using an ANOVA with Bonferroni post-hoc test. Prism (v5.0; GraphPad) was used for data analysis and presentation.

Supplementary Material

Supplementary Material is available at *HMGJ* online.

Acknowledgements

We thank Dr Ernesto Bongarzone (University of Illinois at Chicago) for generously providing the *twitcher* mouse colony. We thank Dr Christoph Pröschel for critical comments on the manuscript.

Conflict of Interest statement. None declared.

Funding

National Institutes of Health, F31-NS078911, https://www.nih.gov (NSH); New York State Department of Health, NYS-DOH-C026877, http://www.stemcell.ny.gov (NSH); New York State Department of Health, NYS-DOH-C029557, http://www.stemcell.ny.gov (MN); New York State Department of Health, NYS-DOH-C026877, http://www.stemcell.ny.gov (CJF); Hunter's Hope, http://www.huntershope.org/site/PageServer (MN); Children's Neurobiological Solutions Foundation, http://pediatricbrainfoundation.org (MN); the Legacy of Angels, http://tloaf.org (MN).

References

1. Gibson, G. (2012) Rare and common variants: twenty arguments. *Nat. Rev. Genet.*, **13**, 135–145.
2. Liu, Y., Gibson, J., Wheeler, J., Kwee, L.C., Santiago-Turla, C.M., Akafo, S.K., Lichter, P.R., Gaasterland, D.E., Moroi, S.E., Challa, P. *et al.* (2011) GALC deletions increase the risk of primary open-angle glaucoma: the role of Mendelian variants in complex disease. *PLoS One*, **6**, e27134.
3. Tayebi, N., Walker, J., Stubblefield, B., Orvisky, E., LaMarca, M.E., Wong, K., Rosenbaum, H., Schiffmann, R., Bembi, B. and Sidransky, E. (2003) Gaucher disease with parkinsonian manifestations: does glucocerebrosidase deficiency contribute to a vulnerability to parkinsonism? *Mol. Genet. Metab.*, **79**, 104–109.
4. Mitsui, J., Mizuta, I., Toyoda, A., Ashida, R., Takahashi, Y., Goto, J., Fukuda, Y., Date, H., Iwata, A., Yamamoto, M. *et al.* (2009) Mutations for Gaucher disease confer high susceptibility to Parkinson disease. *Arch. Neurol.*, **66**, 571–576.
5. Anheim, M., Elbaz, A., Lesage, S., Durr, A., Condroyer, C., Viallet, F., Pollak, P., Bonaïti, B., Bonaïti-Pellié, C., Brice, A. *et al.* (2012) Penetrance of Parkinson disease in glucocerebrosidase gene mutation carriers. *Neurology*, **78**, 417–420.
6. Wenger, D.A., Rafi, M.A., Luzi, P., Datto, J. and Costantino-Ceccarini, E. (2000) Krabbe disease: genetic aspects and progress toward therapy. *Mol. Genet. Metab.*, **70**, 1–9.
7. Duchen, L.W., Eicher, E.M., Jacobs, J.M., Scaravilli, F. and Teixeira, F. (1980) Hereditary leucodystrophy in the mouse: the new mutant twitcher. *Brain*, **103**, 695–710.
8. Farfel-Becker, T., Vitner, E.B. and Futerman, A.H. (2011) Animal models for Gaucher disease research. *Dis. Model Mech.*, **4**, 746–752.
9. Sawcer, S., Hellenthal, G., Pirinen, M., Spencer, C.C., Patsopoulos, N.A., Moutsianas, L., Dilthey, A., Su, Z., Freeman, C., Hunt, S.E. *et al.* (2011) Genetic risk and a primary role for cell-mediated immune mechanisms in multiple sclerosis. *Nature*, **476**, 214–219.
10. Sawcer, S., Franklin, R.J. and Ban, M. (2014) Multiple sclerosis genetics. *Lancet Neurol.*, **13**, 700–709.
11. George, M.F., Briggs, F.B., Shao, X., Gianfrancesco, M.A., Kockum, I., Harbo, H.F., Celius, E.G., Bos, S.D., Hedström, A., Shen, L. *et al.* (2016) Multiple sclerosis risk loci and disease severity in 7,125 individuals from 10 studies. *Neurol. Genet.*, **2**, e87.
12. Barcellos, L.F., Sawcer, S., Ramsay, P.P., Baranzini, S.E., Thomson, G., Briggs, F., Cree, B.C., Begovich, A.B., Villoslada, P., Montalban, X. *et al.* (2006) Heterogeneity at the HLA-DRB1 locus and risk for multiple sclerosis. *Hum. Mol. Genet.*, **15**, 2813–2824.
13. Jokubaitis, V.G. and Butzkueven, H. (2016) A genetic basis for multiple sclerosis severity: Red herring or real? *Mol. Cell. Probes*, **30**, 357–365.
14. Bashinskaya, V.V., Kulakova, O.G., Boyko, A.N., Favorov, A.V. and Favorova, O.O. (2015) A review of genome-wide association studies for multiple sclerosis: classical and hypothesis-driven approaches. *Hum. Genet.*, **134**, 1143–1162.
15. (2014) ACTRIMS-ECTRIMS MSBoston 2014: Late breaking news poster session. *Mult. Scler.*, **20**, 501–510.
16. Wenger, D.A., Sattler, M. and Hiatt, W. (1974) Globoid cell leukodystrophy: deficiency of lactosyl ceramide beta-galactosidase. *Proc. Natl. Acad. Sci. U. S. A*, **71**, 854–857.
17. Wenger, D.A., Rafi, M.A. and Luzi, P. (1997) Molecular genetics of Krabbe disease (globoid cell leukodystrophy): diagnostic and clinical implications. *Hum. Mutat.*, **10**, 268–279.

18. Tomás, J., Durães, J., Lacerda, L. and Macário, M.C. (2015) Adolescent-onset Krabbe disease with an initial diagnosis of multiple sclerosis and a novel mutation. *B.M.J. Case Rep.*, 2015.
19. Suzuki, K. (2003) Globoid cell leukodystrophy (Krabbe's disease): update. *J. Child Neurol.*, **18**, 595–603.
20. Folts, C.J., Scott-Hewitt, N., Pröschel, C., Mayer-Pröschel, M. and Noble, M. (2016) Lysosomal re-acidification prevents lysosphingolipid-induced lysosomal impairment and cellular toxicity. *PLoS Biol.*, **14**, e1002583.
21. Dutta, R. and Trapp, B.D. (2014) Relapsing and progressive forms of multiple sclerosis: insights from pathology. *Curr. Opin. Neurol.*, **27**, 271–278.
22. Voss, E.V., Škuljec, J., Gudi, V., Skripuletz, T., Pul, R., Trebst, C. and Stangel, M. (2012) Characterisation of microglia during de- and remyelination: can they create a repair promoting environment? *Neurobiol. Dis.*, **45**, 519–528.
23. Mahad, D.H., Trapp, B.D. and Lassmann, H. (2015) Pathological mechanisms in progressive multiple sclerosis. *Lancet Neurol.*, **14**, 183–193.
24. Ontaneda, D., Thompson, A.J., Fox, R.J. and Cohen, J.A. (2016) Progressive multiple sclerosis: prospects for disease therapy, repair, and restoration of function. *Lancet*, **pii:** S0140-6736, 31320-31324
25. Kuhlmann, T., Miron, V., Cui, Q., Cuo, Q., Wegner, C., Antel, J. and Brück, W. (2008) Differentiation block of oligodendroglial progenitor cells as a cause for remyelination failure in chronic multiple sclerosis. *Brain*, **131**, 1749–1758.
26. Harlow, D.E., Honce, J.M. and Miravalle, A.A. (2015) Remyelination therapy in multiple sclerosis. *Front. Neurol.*, **6**, 257.
27. Kipp, M., Clarner, T., Dang, J., Copray, S. and Beyer, C. (2009) The cuprizone animal model: new insights into an old story. *Acta Neuropathol.*, **118**, 723–736.
28. Kondo, Y., Adams, J.M., Vanier, M.T. and Duncan, I.D. (2011) Macrophages counteract demyelination in a mouse model of globoid cell leukodystrophy. *J. Neurosci.*, **31**, 3610–3624.
29. Praet, J., Guglielmetti, C., Berneman, Z., Van der Linden, A. and Ponsaerts, P. (2014) Cellular and molecular neuropathology of the cuprizone mouse model: clinical relevance for multiple sclerosis. *Neurosci. Biobehav. Rev.*, **47**, 485–505.
30. Gudi, V., Gingele, S., Skripuletz, T. and Stangel, M. (2014) Glial response during cuprizone-induced de- and remyelination in the CNS: lessons learned. *Front. Cell. Neurosci.*, **8**, 73.
31. Matsushima, G.K. and Morell, P. (2001) The neurotoxicant, cuprizone, as a model to study demyelination and remyelination in the central nervous system. *Brain Pathol.*, **11**, 107–116.
32. Evangelou, N., Konz, D., Esiri, M.M., Smith, S., Palace, J. and Matthews, P.M. (2000) Regional axonal loss in the corpus callosum correlates with cerebral white matter lesion volume and distribution in multiple sclerosis. *Brain*, **123**, (Pt 1845–1849.
33. Kotter, M.R., Li, W.W., Zhao, C. and Franklin, R.J. (2006) Myelin impairs CNS remyelination by inhibiting oligodendrocyte precursor cell differentiation. *J. Neurosci.*, **26**, 328–332.
34. Lampron, A., Larochelle, A., Laflamme, N., Préfontaine, P., Plante, M.M., Sánchez, M.G., Yong, V.W., Stys, P.K., Tremblay, M. and Rivest, S. (2015) Inefficient clearance of myelin debris by microglia impairs remyelinating processes. *J. Exp. Med.*, **212**, 481–495.
35. Matsuo, A., Lee, G.C., Terai, K., Takami, K., Hickey, W.F., McGeer, E.G. and McGeer, P.L. (1997) Unmasking of an unusual myelin basic protein epitope during the process of myelin degeneration in humans: a potential mechanism for the generation of autoantigens. *Am. J. Pathol.*, **150**, 1253–1266.
36. Ihara, M., Polvikoski, T.M., Hall, R., Slade, J.Y., Perry, R.H., Oakley, A.E., Englund, E., O'Brien, J.T., Ince, P.G. and Kalaria, R.N. (2010) Quantification of myelin loss in frontal lobe white matter in vascular dementia, Alzheimer's disease, and dementia with Lewy bodies. *Acta Neuropathol.*, **119**, 579–589.
37. Napoli, I. and Neumann, H. (2010) Protective effects of microglia in multiple sclerosis. *Exp. Neurol.*, **225**, 24–28.
38. Zhang, Y., Chen, K., Sloan, S.A., Bennett, M.L., Scholze, A.R., O'Keeffe, S., Phatnani, H.P., Guarnieri, P., Caneda, C., Ruderisch, N. *et al.* (2014) An RNA-sequencing transcriptome and splicing database of glia, neurons, and vascular cells of the cerebral cortex. *J. Neurosci.*, **34**, 11929–11947.
39. Ito, D., Imai, Y., Ohsawa, K., Nakajima, K., Fukuuchi, Y. and Kohsaka, S. (1998) Microglia-specific localisation of a novel calcium binding protein, Iba1. *Brain Res. Mol. Brain Res.*, **57**, 1–9.
40. Arnett, H.A., Wang, Y., Matsushima, G.K., Suzuki, K. and Ting, J.P. (2003) Functional genomic analysis of remyelination reveals importance of inflammation in oligodendrocyte regeneration. *J. Neurosci.*, **23**, 9824–9832.
41. Olah, M., Amor, S., Brouwer, N., Vinet, J., Eggen, B., Biber, K. and Boddeke, H.W. (2012) Identification of a microglia phenotype supportive of remyelination. *Glia*, **60**, 306–321.
42. Poliani, P.L., Wang, Y., Fontana, E., Robinette, M.L., Yamanishi, Y., Gilfillan, S. and Colonna, M. (2015) TREM2 sustains microglial expansion during aging and response to demyelination. *J. Clin. Invest.*, **125**, 2161–2170.
43. Cantoni, C., Bollman, B., Licastro, D., Xie, M., Mikesell, R., Schmidt, R., Yuede, C.M., Galimberti, D., Olivecrona, G., Klein, R.S. *et al.* (2015) TREM2 regulates microglial cell activation in response to demyelination in vivo. *Acta Neuropathol.*, **129**, 429–447.
44. Rotshenker, S. (2003) Microglia and macrophage activation and the regulation of complement-receptor-3 (CR3/MAC-1)-mediated myelin phagocytosis in injury and disease. *J. Mol. Neurosci.*, **21**, 65–72.
45. Lee, J.K. and Tansey, M.G. (2013) Microglia isolation from adult mouse brain. *Methods Mol. Biol.*, **1041**, 17–23.
46. Macia, E., Ehrlich, M., Massol, R., Boucrot, E., Brunner, C. and Kirchhausen, T. (2006) Dynasore, a cell-permeable inhibitor of dynamin. *Dev. Cell*, **10**, 839–850.
47. Kirchhausen, T., Macia, E. and Pelish, H.E. (2008) Use of dynasore, the small molecule inhibitor of dynamin, in the regulation of endocytosis. *Methods Enzymol.*, **438**, 77–93.
48. Kukita, Y., Furuya, H., Kobayashi, T., Sakai, N. and Hayashi, K. (1997) Characterization of the GALC gene in three Japanese patients with adult-onset Krabbe disease. *Genet. Test*, **1**, 217–223.
49. Tappino, B., Biancheri, R., Mort, M., Regis, S., Corsolini, F., Rossi, A., Stroppiano, M., Lualdi, S., Fiumara, A., Bembi, B. *et al.* (2010) Identification and characterization of 15 novel GALC gene mutations causing Krabbe disease. *Hum. Mutat.*, **31**, E1894–E1914.
50. Kipp, M. (2016) Remyelination strategies in multiple sclerosis: a critical reflection. *Expert Rev. Neurother.*, **16**, 1–3.
51. Franklin, R.J., ffrench-Constant, C., Edgar, J.M. and Smith, K.J. (2012) Neuroprotection and repair in multiple sclerosis. *Nat. Rev. Neurol.*, **8**, 624–634.
52. Paolicelli, R.C., Bolasco, G., Pagani, F., Maggi, L., Scianni, M., Panzanelli, P., Giustetto, M., Ferreira, T.A., Guiducci, E.,

Dumas, L. *et al*. (2011) Synaptic pruning by microglia is necessary for normal brain development. *Science*, **333**, 1456–1458.
53. Hong, S., Dissing-Olesen, L. and Stevens, B. (2016) New insights on the role of microglia in synaptic pruning in health and disease. *Curr. Opin. Neurobiol.*, **36**, 128–134.
54. Piccio, L., Buonsanti, C., Mariani, M., Cella, M., Gilfillan, S., Cross, A.H., Colonna, M. and Panina-Bordignon, P. (2007) Blockade of TREM-2 exacerbates experimental autoimmune encephalomyelitis. *Eur. J. Immunol.*, **37**, 1290–1301.
55. Takahashi, K., Prinz, M., Stagi, M., Chechneva, O. and Neumann, H. (2007) TREM2-transduced myeloid precursors mediate nervous tissue debris clearance and facilitate recovery in an animal model of multiple sclerosis. *PLoS Med.*, **4**, e124.
56. Neumann, H. and Takahashi, K. (2007) Essential role of the microglial triggering receptor expressed on myeloid cells-2 (TREM2) for central nervous tissue immune homeostasis. *J. Neuroimmunol.*, **184**, 92–99.
57. Takahashi, K., Rochford, C.D. and Neumann, H. (2005) Clearance of apoptotic neurons without inflammation by microglial triggering receptor expressed on myeloid cells-2. *J. Exp. Med.*, **201**, 647–657.
58. Xiang, X., Werner, G., Bohrmann, B., Liesz, A., Mazaheri, F., Capell, A., Feederle, R., Knuesel, I., Kleinberger, G. and Haass, C. (2016) TREM2 deficiency reduces the efficacy of immunotherapeutic amyloid clearance. *EMBO Mol. Med.*, **8**, 992–1004.
59. Lue, L.F., Schmitz, C. and Walker, D.G. (2015) What happens to microglial TREM2 in Alzheimer's disease: Immunoregulatory turned into immunopathogenic? *Neuroscience*, **302**, 138–150.
60. Painter, M.M., Atagi, Y., Liu, C.C., Rademakers, R., Xu, H., Fryer, J.D. and Bu, G. (2015) TREM2 in CNS homeostasis and neurodegenerative disease. *Mol. Neurodegener.*, **10**, 43.
61. Jiang, T., Tan, L., Zhu, X.C., Zhang, Q.Q., Cao, L., Tan, M.S., Gu, L.Z., Wang, H.F., Ding, Z.Z., Zhang, Y.D. *et al*. (2014) Upregulation of TREM2 ameliorates neuropathology and rescues spatial cognitive impairment in a transgenic mouse model of Alzheimer's disease. *Neuropsychopharmacology*, **39**, 2949–2962.
62. Rohn, T.T. (2013) The triggering receptor expressed on myeloid cells 2: "TREM-ming" the inflammatory component associated with Alzheimer's disease. *Oxid. Med. Cell Longev*, **2013**, 860959.
63. Jiang, T., Yu, J.T., Zhu, X.C. and Tan, L. (2013) TREM2 in Alzheimer's disease. *Mol. Neurobiol.*, **48**, 180–185.
64. Walter, J. (2016) The triggering receptor expressed on myeloid cells 2: a molecular link of neuroinflammation and neurodegenerative diseases. *J. Biol. Chem.*, **291**, 4334–4341.
65. Wang, Y., Cella, M., Mallinson, K., Ulrich, J.D., Young, K.L., Robinette, M.L., Gilfillan, S., Krishnan, G.M., Sudhakar, S., Zinselmeyer, B.H. *et al*. (2015) TREM2 lipid sensing sustains the microglial response in an Alzheimer's disease model. *Cell*, **160**, 1061–1071.
66. Jay, T.R., Miller, C.M., Cheng, P.J., Graham, L.C., Bemiller, S., Broihier, M.L., Xu, G., Margevicius, D., Karlo, J.C., Sousa, G.L. *et al*. (2015) TREM2 deficiency eliminates TREM2+ inflammatory macrophages and ameliorates pathology in Alzheimer's disease mouse models. *J. Exp. Med.*, **212**, 287–295.
67. Lill, C.M., Rengmark, A., Pihlstrøm, L., Fogh, I., Shatunov, A., Sleiman, P.M., Wang, L.S., Liu, T., Lassen, C.F., Meissner, E. *et al*. (2015) The role of TREM2 R47H as a risk factor for Alzheimer's disease, frontotemporal lobar degeneration, amyotrophic lateral sclerosis, and Parkinson's disease. *Alzheimers Dement.*, **11**, 1407–1416.
68. Wang, Y., Ulland, T.K., Ulrich, J.D., Song, W., Tzaferis, J.A., Hole, J.T., Yuan, P., Mahan, T.E., Shi, Y., Gilfillan, S. *et al*. (2016) TREM2-mediated early microglial response limits diffusion and toxicity of amyloid plaques. *J. Exp. Med.*, **213**, 667–675.
69. Han, J., Wang, M., Ren, M. and Lou, H. (2016) Contributions of triggering-receptor-expressed-on-myeloid-cells-2 to neurological diseases. *Int. J. Neurosci.*, 1–8.
70. Kawabori, M., Kacimi, R., Kauppinen, T., Calosing, C., Kim, J.Y., Hsieh, C.L., Nakamura, M.C. and Yenari, M.A. (2015) Triggering receptor expressed on myeloid cells 2 (TREM2) deficiency attenuates phagocytic activities of microglia and exacerbates ischemic damage in experimental stroke. *J. Neurosci.*, **35**, 3384–3396.
71. Raha, A.A., Henderson, J.W., Stott, S.R., Vuono, R., Foscarin, S., Friedland, R.P., Zaman, S.H. and Raha-Chowdhury, R. (2017) Neuroprotective Effect of TREM-2 in Aging and Alzheimer's Disease Model. *J. Alzheimers Dis*, **55**, 199–217.
72. Lee, J.H., Cho, M.H., Hersh, C.P., McDonald, M.L., Wells, J.M., Dransfield, M.T., Bowler, R.P., Lynch, D.A., Lomas, D.A., Crapo, J.D. *et al*. (2015) IREB2 and GALC are associated with pulmonary artery enlargement in chronic obstructive pulmonary disease. *Am. J. Respir. Cell. Mol. Biol.*, **52**, 365–376.
73. Marshall, M.S. and Bongarzone, E.R. (2016) Beyond Krabbe's disease: The potential contribution of galactosylceramidase deficiency to neuronal vulnerability in late-onset synucleinopathies. *J. Neurosci. Res.*, **94**, 1328–1332.
74. Hawkins-Salsbury, J.A., Shea, L., Jiang, X., Hunter, D.A., Guzman, A.M., Reddy, A.S., Qin, E.Y., Li, Y., Gray, S.J., Ory, D.S. *et al*. (2015) Mechanism-based combination treatment dramatically increases therapeutic efficacy in murine globoid cell leukodystrophy. *J. Neurosci.*, **35**, 6495–6505.
75. Lin, D.S., Hsiao, C.D., Liau, I., Lin, S.P., Chiang, M.F., Chuang, C.K., Wang, T.J., Wu, T.Y., Jian, Y.R., Huang, S.F. *et al*. (2011) CNS-targeted AAV5 gene transfer results in global dispersal of vector and prevention of morphological and function deterioration in CNS of globoid cell leukodystrophy mouse model. *Mol. Genet. Metab.*, **103**, 367–377.
76. Li, Y. and Sands, M.S. (2014) Experimental therapies in the murine model of globoid cell leukodystrophy. *Pediatr. Neurol.*, **51**, 600–606.
77. Liu, J., Lu, W., Guha, S., Baltazar, G.C., Coffey, E.E., Laties, A.M., Rubenstein, R.C., Reenstra, W.W. and Mitchell, C.H. (2012) Cystic fibrosis transmembrane conductance regulator contributes to reacidification of alkalinized lysosomes in RPE cells. *Am. J. Physiol. Cell. Physiol.*, **303**, C160–C169.
78. Bielawski, J., Pierce, J.S., Snider, J., Rembiesa, B., Szulc, Z.M. and Bielawska, A. (2009) Comprehensive quantitative analysis of bioactive sphingolipids by high-performance liquid chromatography-tandem mass spectrometry. *Methods Mol. Biol.*, **579**, 443–467.